Metals and Materials International (2021) 27:1483–1492
https://doi.org/10.1007/s12540-019-00588-6

Effect of Mn Modification on Microstructure and Mechanical Properties of Magnesium Alloy with Low Gd Content

Dongdong Gu[1] · Jian Peng[1,2] · Jiawen Wang[1] · Fusheng Pan[1,2]

Received: 18 September 2019 / Accepted: 17 December 2019 / Published online: 8 January 2020

Abstract
The evolution of microstructure and mechanical properties of the dilute Mg–Gd alloy with Mn modification were investigated systematically in this paper. The results show that the combination of Mn and different processing states could adjust the solid solubility of Gd in the Mg matrix, thereby changing the morphology of the second phases and improving the properties of the alloy. With the addition of 0.8 wt% Mn into the Mg–4Gd alloy, the atomic utilization ratio of Gd atoms decreases from 61.5 to 51.8% during the water-cooling casting process, but it increases from 73.8 to 81.0% during homogenization treatment and increases from 72.3 to 84.1% during hot extrusion. Thus, the mean diameter of granular phases of the Mg–4Gd alloy is larger than that of Mg–4Gd–0.8Mn alloy after the isothermal heat treatment. The Mn addition has little effect on the Hall–Petch constant K_Y and K_H of Mg–4Gd alloy, but improves the σ_0 value significantly due to the increase of the atomic utilization ratio of Gd atoms. Mn element can improve the mechanical properties of Mg–4Gd alloy, and the increase of yield strength and ductility of as-extruded Mg–4Gd–0.8Mn alloy is mainly attributed to grain refinement and the decrease of the texture intensity.

Keywords Mn · Morphology evolution · Atomic utilization ratio · Dilute Mg–Gd alloy · Hall–Petch constant

1 Introduction

Mg alloys have the characteristics of low density, high specific strength, and good machinability, etc., and there is a growing interest in applying it in many fields [1–3]. Especially, Mg–Gd-based alloys have become a hot research topic due to their excellent mechanical properties and corrosion resistance at low, medium and high temperatures [4–8]. However, these advantages can only be brought into full play when the amount of Gd addition is enough. That is to say, if the solid solution utilization efficiency of Gd atoms can be further increased in the magnesium alloys with limited Gd addition, the unit cost of performance of Gd atom can be significantly reduced.

✉ Jian Peng
jpeng@cqu.edu.cn

[1] State Key Laboratory of Mechanical Transmissions, College of Materials Science and Engineering, Chongqing University, Chongqing 400044, China

[2] Chongqing Research Center for Advanced Materials, Chongqing Academy of Science and Technology, Chongqing 401123, China

Manganese, as a traditional alloying element, can be found in the alloy brand standard of lots of commercial magnesium alloys due to its alloying and purification purposes [9, 10]. The solid solubility of Mn in the Mg matrix is low (0.98 at% at 650 °C) according to the Mg–Mn phase diagram [11]. Lai [12] reported that the precipitation process of Mn is rapid and can be completed within 5 min at a temperature higher than 450 °C. Thus, the addition of Mn can provide more displacement sites for the solid solution process of other elements under certain conditions. Moreover, the Mn particles can drag the grain boundary and inhibit DRXed grain growth during the process of deformation, ultimately increasing the strength of the alloy. However, the effect of Mn addition on the solid solubility of Gd in Mg–Gd alloy is seldom studied. The studies have shown that the grain size has a significant effect both on hardness and yield strength of the alloy material [13], and the Hall–Petch constant is strongly affected by crystal type [14] and solid solute atoms [15]. The addition of Gd has been proven to have a significant effect on the Hall–Petch constant for yield strength by Devarajan [16]. Nevertheless, the influence of a small amount of Gd solute (or addition together with Mn solute) on the hardness has rarely been studied.

In this study, the effect of Mn modification on the evolution of microstructure and properties of alloy with limited Gd addition during the water-cooling casting, homogenization, and hot extrusion was investigated systematically. Furthermore, changes in the atomic utilization ratio of Gd in the Mg matrix under different states, and corresponding changes in the Hall–Petch constant for hardness and yield strength were analyzed.

2 Materials and Methods

The alloy ingots were prepared from high-purity Mg (99.99%, mass fraction), Mg–25Gd (wt%) master alloy and Mg–3.25Mn (wt%) master alloy by fabricating in a low carbon steel crucible under a mixed protective gas consisting of SF_6 and CO_2 (1:100). After the melt holding at 720 °C for 30 min, the crucible was quenched in cold water to get a solidified bar. The actual chemical compositions of Mg–Gd (–Mn) alloy were determined by ICP-AES (Inductively-Coupled Plasma/Atomic Emission Spectroscopy), as listed in Table 1. The size of the obtained casting ingot was φ82 mm × 250 mm (diameter × length), and the ingot prepared for extrusion was turned and cut to φ80 mm × 80 mm to remove the oxide scale. The machined ingot was subsequently homogenized at 350 °C for 6 h and followed by 510 °C for 18 h and cooled in air. After that, the ingots were extruded at 430 °C to produce a final sheet with a size of 5 mm in thickness and 60 mm in width, respectively.

The samples for microstructural observation were wet ground to a 1200 grit-finish by a SiC paper gradually and etched using with an etchant (As-cast alloys: alcohol solution containing 4% nitric acid; As-extruded alloys: 5 mL acetic acid, 30 mL anhydrous ethanol and an appropriate amount of picric), and then characterized by optical microscope (OPTEC, MDS) and scanning electron microscope (SEM, Tescan Vega 3 LMH) equipped with energy dispersive X-ray spectroscopy (EDS). Phase constituent and the macro-texture were determined by X-ray diffraction (XRD, Rigaku D/Max 2500) with Cu Kα radiation, a voltage of 40 kV and a current of 100 mA. Vickers hardness tests were carried out with a load of 100 g load and a dwelling time of 15 s. The average grain size was measured by Image Proplus 6.0 software. Tensile specimens were cut from as-cast, as-homogenized, and the extruded sheet parallel to the extrusion direction according to the standard of GB/T 228-2002. Tensile testing was performed on the CMT5105 omnipotent tensile machine at room temperature with a strain rate of 2 mm/min.

Table 1 The actual chemical compositions of Mg–4Gd (–0.8Mn) alloy

Nominal composition (wt%)	Actual composition (wt%)		
	Gd	Mn	Mg
Mg–4Gd	4.13	0	Bal.
Mg–4Gd–0.8Mn	3.99	0.88	Bal.

3 Results

3.1 Microstructures

The optical microstructure and SEM images of the as-cast Mg–4Gd (–0.8Mn) alloy are shown in Fig. 1. It is shown that the matrix of as-cast samples all consist of the typical dendritic α-Mg phase, and the variations of dendrite spacing is negligible even if the 0.8 wt% Mn is added. The average grain size of as-cast Mg–4Gd and Mg–4Gd–0.8Mn alloy is 1019.3 μm and 985.0 μm, respectively. During the solidification process, the particles containing Mn precipitate preferentially and accumulate at the front end of the solid/liquid interface, which is advantageous for hindering grain growth and refining the microstructure of the as-cast alloy. The second phases of Mg–4Gd alloy specimen are sparse and exhibit several different morphologies, mainly including granular phases and continuous irregular-laths-like phases (see in Fig. 1a, b). The second phase of Mg–4Gd–0.8Mn alloy is coarsened obviously, and the distribution of them becomes more glomerate with some of them in a lamellae structure (see in Fig. 1d, e). It is easy to find that the mean diameter of the granular phases in as-cast Mg–4Gd alloy is smaller than that of as-cast Mg–4Gd–0.8Mn alloy. Besides that, the volume fraction of the second phases in Mg–4Gd–0.8Mn alloy (1.18%) is much larger than that of Mg–4Gd alloy (0.40%), indicating that the addition of Mn promotes the formation and growth of the second phase. EDS line scanning is employed to analyze element concentration trends. The intensity of the Gd element in as-cast Mg–4Gd alloy reaches the peak value at the white area (see in Fig. 1c), while both Gd and Mn elements in as-cast Mg–4Gd–0.8Mn alloy reach the peak intensity at the same site (see in Fig. 1f). That indicates that Mn atoms may be dissolved in the MgGd phase or participate in the formation of the MgGd phase.

The XRD pattern and analysis result of as-cast Mg–4Gd (–0.8Mn) alloy are shown in Fig. 2, indicating that the addition of Mn element does not lead to the formation of any new phases with Mg or Gd. However, the intensity of diffraction peak of Mg_5Gd phase increases due to the addition of Mn, meaning that Mn element can promote the formation of the Mg_5Gd phase during the water-cooling casting process.

The optical microstructure, SEM images, and EDS results of as-homogenized Mg–4Gd (–0.8Mn) alloy are shown in Fig. 3. After homogenization treatment, the average grain

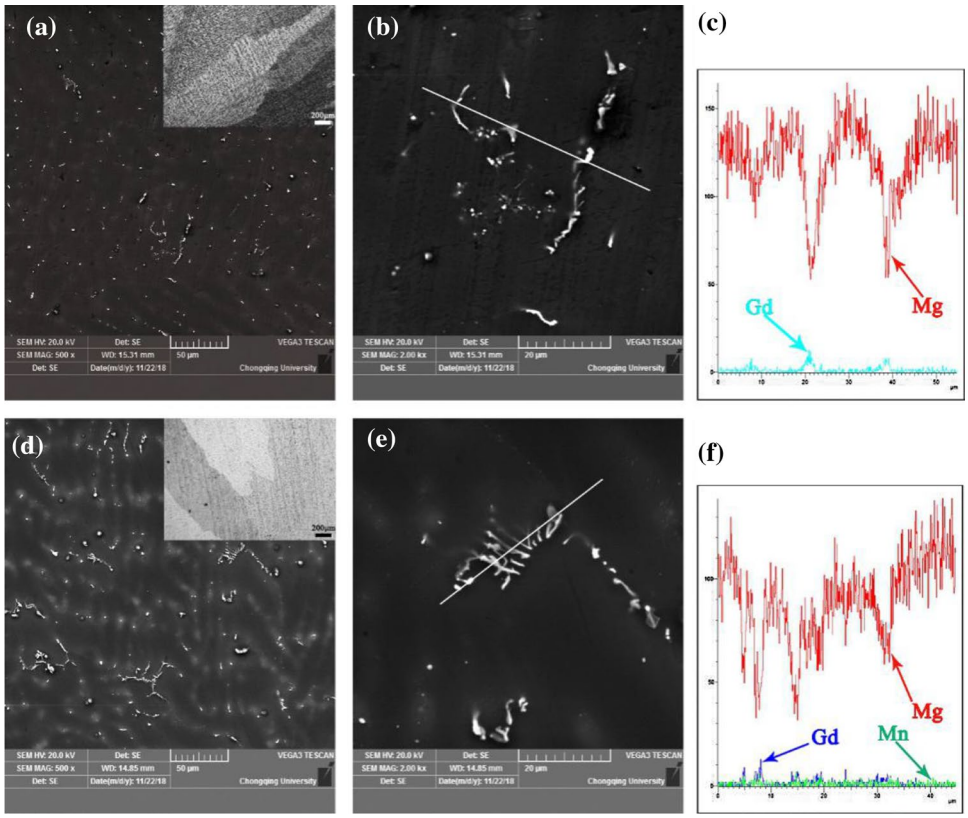

Fig. 1 Optical microstructure, SEM images, and EDS line scanning results of as-cast samples: **a–c** Mg–4Gd alloy; **d–f** Mg–4Gd–0.8Mn alloy

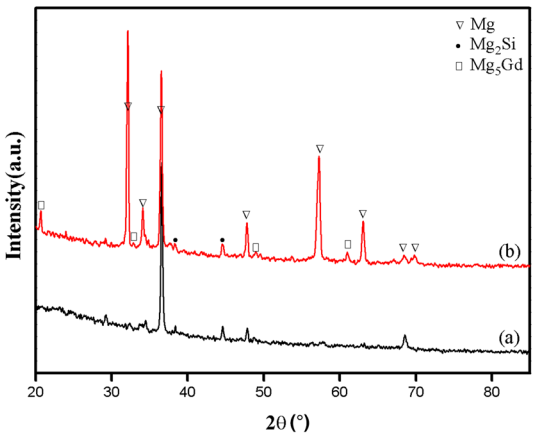

Fig. 2 XRD pattern and analysis result of as-cast alloys: **a** Mg–4Gd alloy; **b** Mg–4Gd–0.8Mn alloy

size of the as-homogenized Mg–4Gd and Mg–4Gd–0.8Mn alloys increases to 1445.8 and 1362.5 μm, respectively. Needle-like (mean length of 2.36 μm, mean width of 0.35 μm) phases parallel to each other and irregular granular (mean diameter of 2.14 μm) phases can be observed obviously in Mg–4Gd alloy (see in Fig. 3a, b). Based on the analysis of SEM–EDS, the needle-like phase (S2) is considered as GdH_2, which is consistent with the previous reports [17–19]. The smaller irregular granular phase (S3) consisting of Mg and Gd elements may be deemed as Mg_5Gd phase (atom ratio of Mg and Gd closed to 5:1), and the larger irregular granular phase (S1) is abounded in Gd (or Gd-rich phase) (atom ratio of Mg and Gd closed to 1:2). However, with Mn addition as Mg–4Gd–0.8Mn alloy, the needle-like phases disappear largely, and the mean diameter of the granular phases decreases obviously as 0.70 μm (see in Fig. 3c, d). The irregular granular phase (S4) may also be evaluated as Mg_5Gd phase due to their atom ratio. As for some darker phase with a high concentration of Mn as S5, the Mn atoms may be dissolved in the Mg–Gd phase or participate in the formation of the Mg–Gd phase. By statistic, after homogenization treatment, the area fraction of second phases in Mg–4Gd alloy increases sharply from 0.35 to 1.84%, while it remains nearly constant as 1.22% in Mg–4Gd–0.8Mn alloy. That attributes to the coarsening of second phases, and the increase in solute solubility of Gd by Mn addition during the homogenization treatment.

As shown in Fig. 4, both the as-extruded Mg–4Gd and Mg–4Gd–0.8Mn alloys exhibit homogeneous equiaxed grain structure, indicating fully recrystallization occurs during hot extrusion [20]. Although Mn has no grain refining effect for as-cast Mg–Gd alloy, it can work for refining the extrusion sample. The average grain size of the as-extruded Mg–4Gd and Mg–4Gd–0.8Mn alloy is about 8.54 and 6.54 μm, respectively. The second phases of as-extruded Mg–4Gd alloy distribute along the extrusion direction as extrusion

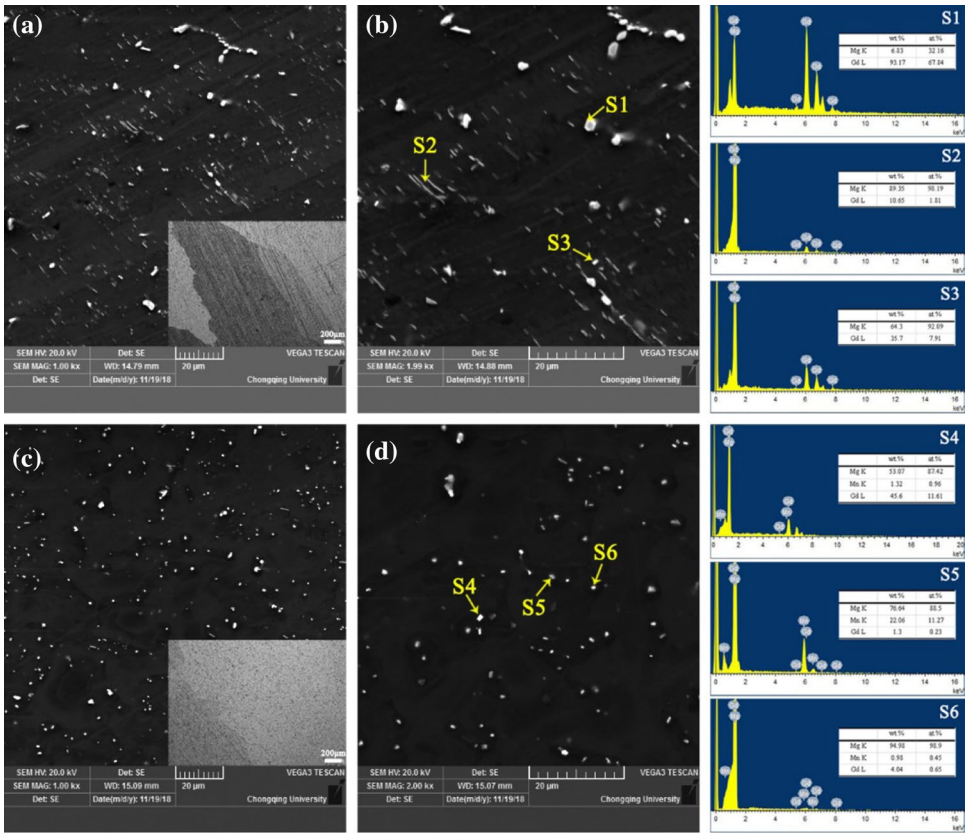

Fig. 3 Optical microstructure, SEM images and EDS results of as-homogenized samples: **a**, **b** Mg–4Gd alloy; **c**, **d** Mg–4Gd–0.8Mn alloy

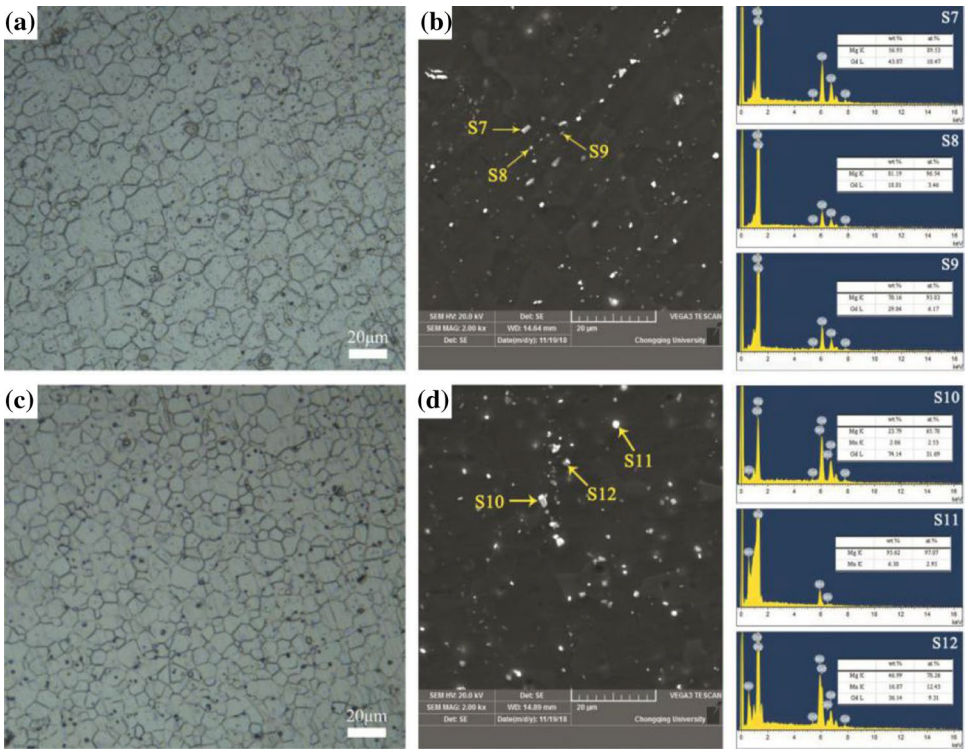

Fig. 4 Optical microstructure, SEM images and EDS results of as-extruded alloy samples: **a**, **b** Mg–4Gd alloy; **c**, **d** Mg–4Gd–0.8Mn alloy

streamlines, which mainly consist of rod-like phases and granular phases (see in Fig. 4b). Based on the analysis of SEM–EDS, the rod-like phases (S7 and S9) are considered as Mg_5Gd phase (atom ratio of Mg and Gd closed to 5:1). Compared with the as-extruded Mg–4Gd alloy, Mn can be observed in some phases of Mg–4Gd–0.8Mn alloy, showing that Mn atoms may be dissolved in the MgGd phase (see in S10–12). By statistic, after the extrusion process, the area fraction of second phases in Mg–4Gd alloy (1.60%) is almost as same as that in the Mg–4Gd–0.8Mn alloy (1.65%).

The X-ray basal pole figures of the as-extruded Mg–4Gd (–0.8Mn) alloy are shown in Fig. 5. The macro-texture data shows that a strong basal texture exists in the as-extruded Mg–4Gd alloy, and the c-axis is tilted away from the ND towards the ED with two basal poles mainly along the ED. Due to the tilted basal poles and the absence of twins, the <a + c> pyramidal slip is needed and is also favorably oriented for the chosen deformation geometry [21]. The activation of <a + c> slip leads to an increasing tendency of basal poles rotate from ND toward ED. Thus, the tilt of basal poles is most likely attributed to the pyramidal <a + c> slip. The peak texture intensity of as-extruded Mg–4Gd alloy reaches 17.0, while it reduces significantly to 7.9 for as-extruded Mg–4Gd–0.8Mn alloy. With the addition of 0.8 wt% Mn, the basal plane of most grains is preferentially parallel to ED, and the off-basal component is gradually reduced. Furthermore, the spread of the basal texture of as-extruded Mg–4Gd–0.8Mn alloy becomes more dispersive. The above results indicate that the addition of 0.8 wt% Mn can be a practical approach to modify the basal texture.

3.2 Mechanical Property

The mechanical properties of as-cast, as-homogenized, and as-extruded Mg–4Gd (–0.8Mn) alloy are shown in Fig. 6. The tensile yield strength (TYS), ultimate tensile strength (UTS), and elongation (EL) of as-cast Mg–4Gd alloy are relatively weak with just 21.53 MPa, 49.53 MPa, and 4.04%, respectively. With 0.8 wt% Mn addition, the TYS, and UTS of the alloy are improved to 31.76 MPa, 72.76 MPa, respectively, while the EL decreases (see in Fig. 6a and Table 2). After homogenization treatment, the strength of Mg–4Gd alloy decreases, but the strength of Mg–4Gd–0.8Mn alloy increases. The TYS, UTS, and EL of as-homogenized Mg–4Gd alloy are improved with 0.8 wt% Mn addition, by about 29 MPa, 74 MPa, and 2.7%,

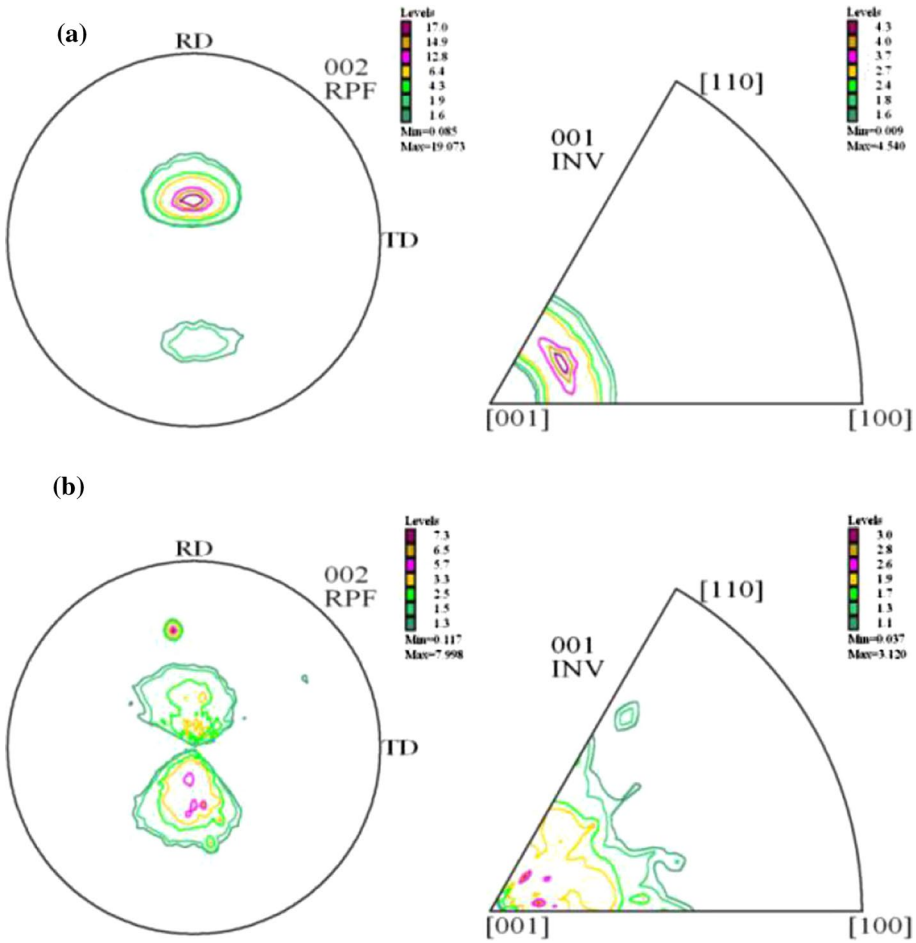

Fig. 5 {0001} pole figures and inverse pole figures of as-extruded alloy **a** Mg–4Gd alloy; **b** Mg–4Gd–0.8Mn alloy

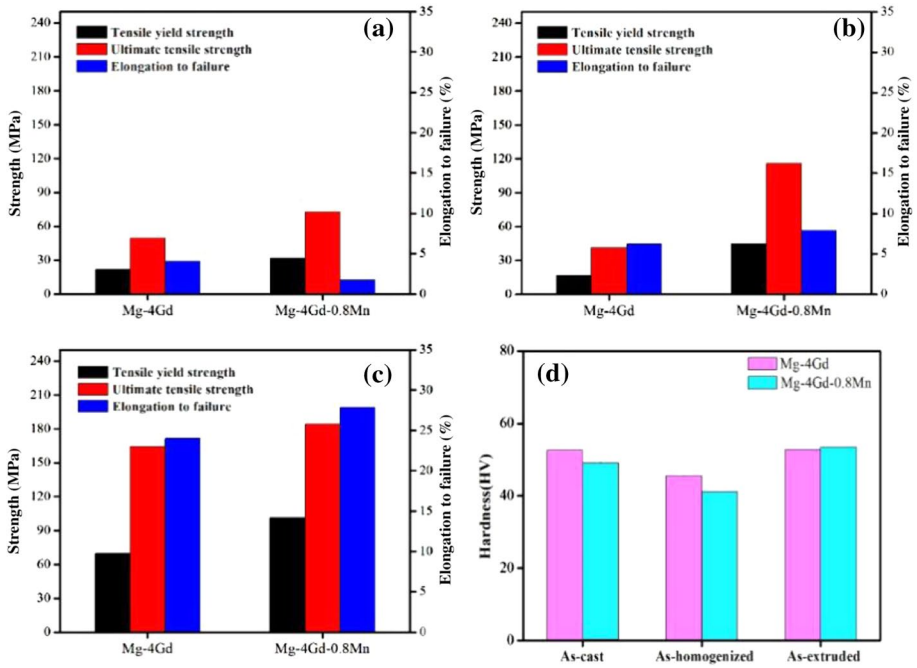

Fig. 6 Mechanical properties of the as-cast **a**, as-homogenized **b** and as-extruded **c** of Mg–Gd(–Mn) alloy and their hardness **d**

Table 2 The summary of the tensile properties and hardness of Mg–4Gd (–0.8Mn) alloy

	TYS (MPa)	UTS (MPa)	EL (%)	Hardness (HV)
As-cast Mg–4Gd alloy	21.53	49.53	4.04	52.58
As-cast Mg–4Gd–0.8Mn alloy	31.76	72.76	1.74	49.07
As-homogenized Mg–4Gd alloy	16.82	41.51	6.23	45.50
As-homogenized Mg–4Gd–0.8Mn alloy	45.03	115.90	7.91	41.10
As-extruded Mg–4Gd alloy	69.41	164.55	24.00	52.78
As-extruded Mg–4Gd–0.8Mn alloy	101.33	184.00	27.82	53.37

respectively (see in Fig. 6b and Table 2). After hot extrusion, both the Mg–4Gd and Mg–4Gd–0.8Mn alloys exhibit the best tensile properties (see in Fig. 6c and Table 2). The TYS, UTS, and EL of the as-extruded Mg–4Gd alloy are only 69.41 MPa, 164.55 MPa, and 24.00%, respectively. However, with the 0.8 wt% Mn addition, the alloy exhibits a TYS of 101.33 MPa with an increment of about 46.0%, a UTS of 184.00 MPa with an increment of about 11.8%, and an elongation to failure of 27.82% with an increment of about 15.9%. All of these indicate that the Mn element can improve the tensile properties of Mg–4Gd alloy.

Figure 6d shows the hardness values of the as-cast, as-homogenized, and as-extruded Mg–4Gd (–0.8Mn) alloy. The hardness of as-cast Mg–4Gd alloy is 52.58 HV, and it decreases to 45.50 HV after the homogenization and increases to 52.78 HV after extrusion. But with the addition of 0.8 wt% Mn, the hardness values of as-cast and as-homogenized samples decrease by 6.7% (49.07 HV) and 9.7% (41.10 HV), respectively. The hardness of as-homogenized Mg–4Gd (–0.8Mn) alloy decreases for the significant coarsening of the grain. Conversely, after hot extrusion, the hardness of them increases for grain refinement. Besides, the hardness of as-extruded Mg–4Gd–0.8Mn alloy is slightly larger than that of as-extruded Mg–4Gd alloy, indicating that Mn has a positive effect on the improvement of hardness.

4 Discussion

4.1 Morphology Evolution of the Second Phase and Variation in Solid Solubility of Gd

The schematic diagram of the morphology evolution of the second phase is shown in Fig. 7. It indicates that the morphology of the second phase can be modified by combining Mn with different processing states. Mn has a negligible effect on grain size of as-cast Mg–Gd alloy for its relatively lower growth restriction factor (GRF) [22, 23] in magnesium alloy, while it has a significant effect on the morphology of the second phases (see in Figs. 2 and 7). An EDS analysis of more than twenty points is performed for each sample to identify the solute solubility of Gd in the alloy matrix (or

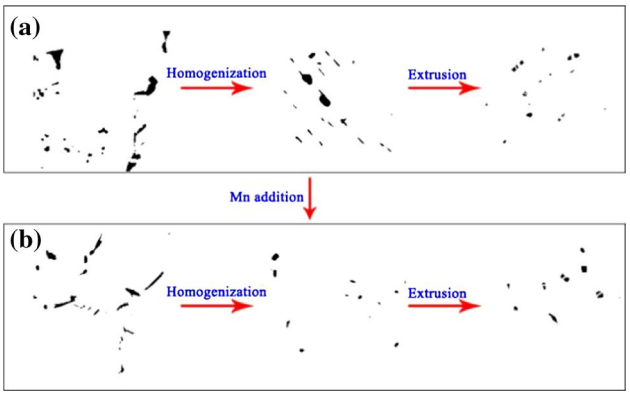

Fig. 7 Schematic diagram of morphology evolution of the second phases: **a** Mg–4Gd alloy and **b** Mg–4Gd–0.8Mn alloy

called atomic utilization ratio), and the results are shown in Fig. 8 and Table 2. Mn can increase the volume fraction of the second phases in the as-cast alloy, due to the higher supersaturation solubility of Mn and the decrease of atomic utilization ratio of Gd from 61.5 to 50.8% during the water-cooling casting process.

During the homogenization treatment of as-cast Mg–Gd (–0.8Mn) alloy, the decomposition and precipitation of the second phases in supersaturated solid solution co-occur [24]. The second phases with lamellar structure in as-cast Mg–4Gd alloy gradually transform into short-bar and granular phases (see in Figs. 1a and 3a); the phases in as-cast Mg–4Gd–0.8Mn alloy gradually transform into granular second phases (see in Figs. 1c and 3c). The morphology evolution of the second phases (see in Fig. 7) during the homogenization treatment, meets the rule of the thermodynamic formula for homogeneous nucleation of the second phase,

$$\Delta G_{NUC} = -V\Delta Gv + A\sigma \quad (1)$$

In which ΔG_v is the volume free energy change of the nucleation, σ is the surface energy of the interface between the two phases. A is the surface area of the nucleus, and V is nucleation volume. As it is well known, both the continuous irregular-laths-like phases and the phases in a lamellar structure are unstable. Thus, these morphology change of the phases in as-cast Mg–4Gd (–0.8Mn) alloy can reduce the Gibbs free energy of the system. Moreover, the addition of Mn decreases the volume fraction of short-bar phases of the Mg–Gd alloy, indicating that Mn can accelerate the reduction of the Gibbs free energy.

During the homogenization treatment, some of the Mg_5Gd phases dissolve into the Mg matrix, and some of the Gd-rich phases are left. During isothermal heat treatment, the atomic utilization ratio of Gd in both Mg–4Gd and Mg–4Gd–0.8Mn alloy increases obviously from 61.5 to 73.8% and 50.8 to 81.0%, respectively; and the solid solubility of Mn in Mg–4Gd–0.8Mn alloy decreases from 0.42 to 0.18 at%. The results show that the addition of Mn increases the atomic utilization ratio of Gd in Mg-matrix, and the precipitation process of Mn is not completed, which is different from the report by Lai [12]. The mean diameter of the granular phases in as-homogenized Mg–Gd alloy (2.14 μm) is bigger than that of as-homogenized Mg–Gd alloy (0.70 μm), as shown in Fig. 3a, c, which is following "diffusion and growth" model [25] and Ostwald ripening theory [26]. Since the size of MgGd phases is not uniform, the solute concentration near the small size MgGd phase is higher than that near the big size MgGd phase. Under the driving force from concentration difference, the Gd atoms near the small size MgGd phase will diffuse to the big size MgGd phase directionally. Thus, the smaller size MgGd phases will become less in number, and the big size MgGd phases will become larger in size. However, the addition of 0.8 wt% Mn decreases the atomic utilization ratio of Gd from 61.5 to 50.8% during the water-cooling casting, which leads to the concentration difference around the small size phases in as-cast Mg–4Gd alloy is higher than that in as-cast Mg–4Gd–0.8Mn alloy. Finally, the size of granular phases in as-homogenized Mg–Gd alloy is larger than that in the as-homogenized Mg–4Gd–0.8Mn alloy.

During hot extrusion, the larger second phases are crushed into smaller particles, and the DRX occurs, as indicated in Fig. 5. The average grain size of as-extruded Mg–4Gd alloy is larger than that of as-extruded Mg–4Gd–0.8Mn alloy,

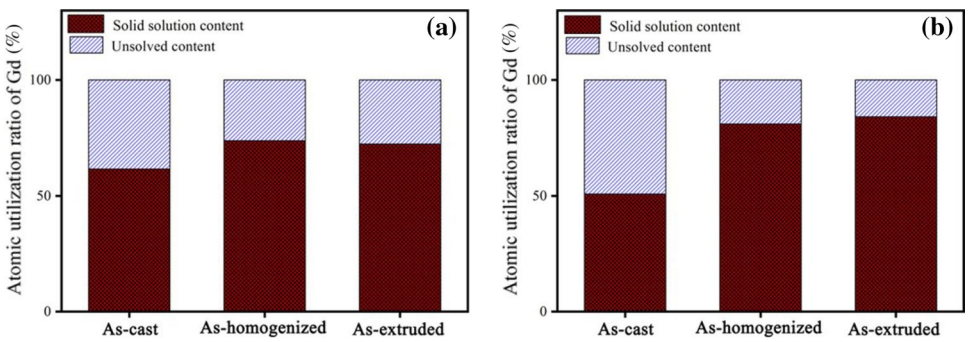

Fig. 8 Variation in solid solubility of Gd in Mg matrix of the alloy specimens: **a** Mg–4Gd alloy and **b** Mg–4Gd–0.8Mn alloy

Table 3 The solid solubility and relative proportion of Gd atom (and Mn atom) in the Mg matrix, and the volume fraction of the second phases (*fv*) of the alloy in different states

	Mg–4Gd alloy		Mg–4Gd–0.8Mn alloy		
	Gd_{Sol}/relative proportion	*fv* (%)	Gd_{Sol}/relative proportion	Mn_{Sol}	*fv* (%)
As-cast	0.40 at%/61.5%	0.35	0.32 at%/50.8%	0.42 at%	1.18
As-homogenized	0.48 at%/73.8%	1.84	0.51 at%/81.0%	0.18 at%	1.22
As-extruded	0.47 at%/72.3%	1.60	0.53 at%/84.1%	0 at%	1.65

indicating that the precipitated Mn particles can act as effective nucleation sites and then accelerate DRX. Furthermore, precipitates can suppress the growth of the DRXed grain [27]. According to Table 3, the atomic utilization ratio of Gd in as-extruded Mg–4Gd alloy decreases slightly from 73.8 to 72.3%, while it still increases in as-extruded Mg–4Gd–0.8Mn alloy from 81.0 to 84.1%. Also, the solid solubility of Mn in Mg–4Gd–0.8Mn alloy decreases from 0.18 to 0 at%, indicating that all the Mn atoms have been precipitated completely during extrusion.

From the above analysis, the solid solubility of Gd in Mg matrix can be regulated by combining the addition of Mn with different processing states, due to the precipitation of Mn atoms from the matrix and then providing more solid solution sites for Gd atoms, which is of considerable significance on precise control of Gd content and its efficient use in practical production.

4.2 Evolution of Hall–Petch Constant and Mechanical Properties

Figure 6 shows the yield strength and hardness value of Mg–4Gd (–0.8Mn) alloy under different treatments. As mentioned earlier, the grain size has a significant effect on the hardness and strength of a polycrystal, which follows the Hall–Petch relationship ($H = H_0 + K_H d^{-1/2}$ *and* $\sigma = \sigma_0 + K_Y d^{-1/2}$, where d is the mean grain size, H_0, σ_0, K_H, and K_Y are appropriate constants that are determined experimentally). As shown in Fig. 9, the hardness of Mg–4Gd (–0.8Mn) alloy exhibits grain size independence. Both the K_H value of Mg–4Gd alloy ($K_H = 0.38$ kg mm$^{-3/2}$) and Mg–4Gd–0.8Mn alloy ($K_H = 0.72$ kg mm$^{-3/2}$) are small and close, indicating that the addition of Mn has a little effect on Hall–Petch constant K_H of dilute Mg–Gd alloy.

Nagarajan [16] reported that Gd in solution has stronger effects on K_Y value. Similarly, the Hall–Petch relation of the studied Mg–4Gd (–0.8Mn) alloy calculated by yield strength and grain size is shown in Fig. 10, and its corresponding value of σ_0 and K_Y are shown in Table 4. The values of σ_0 and K_Y for pure Mg in Table 4 are from Ref. [28]. The K_Y value of Mg–4Gd and Mg–4Gd–0.8Mn alloy are very close, just 0.16 and 0.17 MPa·m$^{-1/2}$, respectively. Furthermore, both of them are lower than that of the pure Mg, which means that

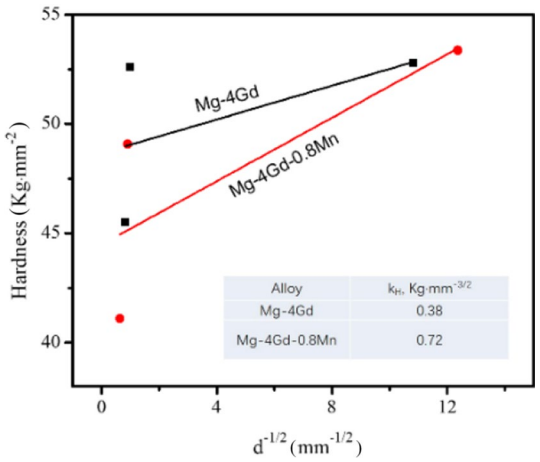

Fig. 9 Variation in Vickers hardness with $d^{-1/2}$ for Mg–4Gd (–0.8Mn) alloy

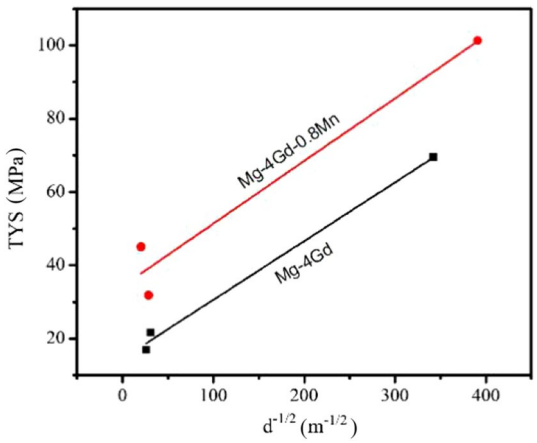

Fig. 10 Hall–Petch content calculation, using TYS data for Mg–4Gd (–0.8Mn) alloy

Table 4 Hall–Petch constant for yield strength of Mg–Gd (–0.8Mn) alloy

Alloy	K_Y, MPam$^{-1/2}$	σ_0, MPa
Pure Mg [28]	0.23	10.06
Mg–4Gd	0.16	14.54
Mg–4Gd–0.8Mn	0.17	34.25

Gd has a limited strengthening effect on dilute alloy. Moreover, it also reflects on the solid solution softening effects [29] of the dilute alloys in comparison with pure Mg, which is by making prism slip easier. The σ_0 value of Mg alloy can be related to the critical resolved shear stresses (CRSS) of basal and prism slip, which are changed by solute atoms. Thus, the addition of Mn can improve the σ_0 value by increasing the atomic utilization ratio of Gd in the Mg matrix.

The as-cast Mg–4Gd alloy in this study exhibits relatively low strength, as shown in Fig. 6a, but the Mg–4Gd–0.8Mn alloy exhibits a higher TYS and UTS. The improvement in strength is mainly attributed to solid solution strengthening and dispersion strengthening. Although the solid solubility of Gd decreases slightly in Mg–4Gd–0.8Mn alloy, the water cooling process results in a certain solid solubility of Mn, as shown in Table 2. Moreover, the volume fraction of the second phase in Mg–4Gd–0.8Mn alloy (1.18%) is much larger than that of Mg–4Gd alloy (0.40%).

After the homogenization treatment, the Mg–4Gd alloy exhibits lower TYS and UTS, while the Mg–4Gd–0.8Mn alloy exhibits a higher TYS and UTS, as shown in Fig. 6b. Although the solid solubility of Gd atom and the area fraction of second phases increase, the brittle needle-like phase and large irregular granular phase in the as-homogenized Mg–4Gd alloy, which are easy to induce stress concentration and form microcracks, can provide a negative influence on TYS and UTS. However, with the addition of Mn as Mg–4Gd–0.8Mn alloy, the needle-like phases disappear obviously, and the mean diameter of the granular phases decreases significantly, leading to a significant improvement in strength.

The strength of Mg–4Gd (–0.8Mn) alloy is improved obviously by hot extrusion. The strengthening effect includes the grain refinement, the precipitation of the second phase, and solid solution strengthening. The classic Hall–Patch relation points out that TYS is proportional to $d^{-1/2}$. The addition of Mn decreases the average grain size from 8.54 to 6.54 μm and then improves the TYS of the alloy by grain refinement. The precipitation strengthening is almost the same for nearly the same area fraction of the second phases, as shown in Table 2. The atomic utilization ratio of Gd in as-extruded Mg–4Gd–0.8Mn alloy (84.1%) is higher than that in as-extruded Mg–4Gd alloy (72.3%), indicating that the addition of Mn can increase the solid solution strengthening. Texture is another crucial influencing factor associated closely with strength in magnesium alloys [30]. With 0.8 wt% Mn addition, the intensity of the basal texture of Mg–4Gd alloy reduces significantly, and its spread becomes more dispersive, as shown in Fig. 5. The possible reasons of the weakened texture in Mn-modified samples are related to the solid solubility of Gd element and the varied DRX behavior during the extrusion process compared to that of Mn-free sample. With 0.8 wt% Mn addition, the atomic utilization ratio of Gd increases, which could weaken the basal texture. Another reason can be ascribed to the varied DRX behavior derived from secondary phase particles during the extrusion process. Hence, the effects of thermally stable MgGd phases and Mn particles on DRXed nucleation and the DRXed grain growth should be analyzed. According to the particle-stimulated nucleation (PSN) of recrystallization theory, the size of second-phase particle has a significant effect on DRX nucleation. In other words, large particles (> 1 μm) can act as effective nucleation sites by increasing dislocation density, thereby accelerating DRX, while fine particles (< 1 μm) can induce grain boundary pinning effects and ultimately retard DRX behavior. In this study, the as-extruded Mg–4Gd–0.8Mn alloy has more large size particles (> 1 μm) than that of as-extruded Mg–4Gd alloy (see in Fig. 4). Imandoust et al. [31] reported that the DRXed grains via the PSN mechanism have a relative random orientation and result in a weakening of the overall texture. Meanwhile, it makes most of the grains be in a soft orientation with a low Schmid factor when the tensile direction is along ED. Therefore, the weakening intensity of basal texture in Mg–4Gd–0.8Mn alloy would enhance its ductility. From the above the discussion, it can be concluded that the increase in yield strength and ductility in as-extruded Mg–4Gd–0.8Mn alloy is mainly attributed to the grain refinement and the decreasing of the basal texture intensity.

5 Conclusions

In this study, the evolution of microstructure and mechanical properties of magnesium alloy with Mn modification during the water-cooling casting, homogenization, and hot extrusion were investigated systematically. The main results are summarized as follows:

1. By combining Mn addition with different processing states, the solid solubility of Gd can be controlled to change the morphology of the phase and improve the properties of the alloy. With 0.8 wt% Mn addition, the atomic utilization ratio of Gd atoms decreases from 61.5 to 51.8% during the water-cooling casting process, but it increases from 73.8 to 81.0% during homogenization treatment and increases from 72.3 to 84.1% during hot extrusion.
2. Mn addition has little effect on Hall–Petch constant K_H and K_Y of Mg–4Gd alloy, but the σ_0 value increases significantly with the increase of the atomic utilization ratio of Gd.
3. The strength of Mg–4Gd (–0.8Mn) alloy is improved significantly after hot extrusion. The increase in yield strength and ductility of the as-extruded Mg–4Gd–0.8Mn alloy is mainly attributed to the grain refinement and the decrease of the texture intensity.

Acknowledgements The authors are grateful for the financial supports from the National Key Research and Development Program of China (No. 2016YFB0301100), the Fundamental Research Funds for the Central Universities (No. 2018CDJDCD0001), and the Key Nature Science Foundation of Chongqing (No. cstc2017jcyjBX0040).

Compliance with Ethical Standards

Conflict of interest The authors declare that they have no conflict of interest.

References

1. M. Janbozorgi, K.K. Taheri, A.K. Taheri, J. Magnes. Alloys **7**, 80–89 (2019)
2. S. Khalifeh, T.D. Burleigh, J. Magnes. Alloys **6**, 327–336 (2018)
3. W. Liu, Z.J. Yan, Z.D. Zhang, Y.X. Zhang, G.Y. Cai, Z.Y. Li, J. Alloys Compd. **788**, 705–711 (2019)
4. F. Zhang, Y.F. Wang, Y.B. Duan, K.J. Wang, Y.T. Wang, W.J. Zhang, J. Hu, J. Alloys Compd. **788**, 541–548 (2019)
5. D.J. Chen, K. Zhang, T. Li, X.G. Li, Y.J. Li, M.L. Ma, G.L. Shi, J.W. Yuan, Mater. Sci. Eng. A **744**, 1–9 (2019)
6. J.L. Li, D. Wu, R.S. Chen, E.H. Han, Acta Mater. **159**, 31–45 (2018)
7. J.H. Zhang, S.J. Liu, R.Z. Wu, L.G. Hou, M.L. Zhang, J. Magnes. Alloys **6**, 277–291 (2018)
8. H. Zhou, H.Y. Ning, X.L. Ma, D.D. Yin, L.R. Xiao, X.C. Sha, Y.D. Yu, Q.D. Wang, Y.S. Li, J. Mater. Sci. Technol. **34**, 1067–1075 (2018)
9. X.W. Heng, Y. Zhang, W. Rong, Y.J. Wu, L.M. Peng, Mater. Des. **169**, 107666 (2019)
10. H.-Y. Ha, H.J. Kim, S.-M. Baek, B. Kim, S.-D. Sohn, H.-J. Shin, H.Y. Jeong, S.H. Park, C.D. Yim, B.S. You, J.G. Lee, S.S. Park, Scr. Mater. **109**, 38–43 (2015)
11. H. Okamoto, J. Phase Equilib. Diff. **36**, 390–401 (2015)
12. L. Lai, K. Zhang, X.G. Li, Y.J. Li, M.L. Ma, G.L. Shi, J. Rare Earths **6**, 552–558 (2016)
13. Y. Xu, F. Gensch, Z. Ren, K.U. Kainer, N. Hort, Prog. Nat. Sci. Mater. **28**, 724–730 (2018)
14. N. Ono, R. Nowak, S. Miura, Mater. Lett. **58**, 39–43 (2004)
15. H. Somekawa, T. Mukai, Mater. Sci. Eng. A **561**, 378–385 (2013)
16. D. Nagarajan, C.H. Caceres, J.R. Griffiths, Metall. Mater. Trans. A **47A**, 5401–5408 (2016)
17. M. Vlkek, J. Cizek, F. Lukac, P. Hruska, B. Smola, I. Stulikova, H. Kudrnova, P. Minarik, T. Kmjec, T. Vlasak, Int. J. Hydrogen Energ. **42**, 22598–22604 (2017)
18. K.Y. Zheng, J. Dong, X.Q. Zeng, W.J. Ding, Mater. Sci. Technol. **24**, 320–326 (2008)
19. L. Xiao, G.Y. Yang, Y. Liu, S.F. Luo, W.Q. Jie, J. Mater. Sci. Technol. **34**, 2246–2255 (2018)
20. J.D. Robson, D.T. Henry, B. Davis, Acta Mater. **57**, 2739–2747 (2009)
21. J.R. Dong, D.F. Zhang, Y.F. Dong, S.S. Chai, F.S. Pan, Mater. Sci. Eng. A **618**, 262–270 (2014)
22. Y.C. Lee, A.K. Dahle, D.H. StJohn, Metall. Mater. Trans. A **31**, 2895–2906 (2000)
23. Z. Fan, F. Gao, L. Zhou, S.Z. Lu, Acta Mater. **152**, 248–257 (2018)
24. J.W. Kang, C.J. Wang, K.K. Deng, K.B. Nie, Y. Bai, W.J. Li, J. Alloys Compd. **720**, 196–206 (2017)
25. J.L. Zhang, Y.L. Liu, J. Liu, Y.C. Yu, S.B. Wang, J. Alloys Compd. **663**, 610–616 (2016)
26. B.F. Luan, L.J. Chai, J.W. Chen, M. Zhang, Q. Liu, J. Nucl. Mater. **423**, 127–131 (2012)
27. M.G. Jiang, C. Xu, H. Yan, S.H. Lu, T. Nakata, C.S. Lao, R.S. Chen, S. Kamado, E.H. Han, Sci. Rep-UK 8, 1-11 (2018)
28. D. Nagarajan, C.H. Cáceres, J.R. Griffiths, Metall. Mater. Trans. A **47**, 5401–5408 (2016)
29. A.H. Blake, C.H. Cáceres, Mater. Sci. Eng. A **483–484**, 161–163 (2008)
30. Q.H. Wang, Y.Q. Shen, B. Jiang, A.T. Tang, Y.F. Chai, J.F. Song, T.H. Yang, G.S. Huang, F.S. Pan, Mater. Sci. Eng. A **736**, 404–416 (2018)
31. A. Imandoust, C.D. Barrett, A.L. Oppedal, W.R. Whittington, Y. Paudel, H.E. Kadiri, Acta Mater. **138**, 27–41 (2017)